Vibration−Rotation Energy Pattern in Acetylene: $^{13}CH^{12}CH$ up to 10 120 cm^{-1}†

S. Robert,[#,‡] B. Amyay,[⊥,‡] A. Fayt,[§] G. Di Lonardo,[||] L. Fusina,[||] F. Tamassia,[||] and M. Herman*[,‡]

Service de Chimie Quantique et Photophysique CP160/09, Faculté des Sciences, Université Libre de Bruxelles, Av. Roosevelt, 50, B-1050 Bruxelles, Belgium, Laboratoire de Spectroscopie Moléculaire, Université Catholique de Louvain, Chemin du Cyclotron, 2, B-1348 Louvain-La-Neuve, Belgium, and Dipartimento di Chimica Fisica e Inorganica, Università di Bologna, Viale Risorgimento, 4, I-40136 Bologna, Italy

Received: April 30, 2009; Revised Manuscript Received: June 15, 2009

All 18 219 vibration−rotation absorption lines of $^{13}CH^{12}CH$ published in the literature, accessing substates up to 9400 cm^{-1} and including some newly assigned, were simultaneously fitted to *J*-dependent Hamiltonian matrices exploiting the well-known vibrational polyad or cluster block-diagonalization, in terms of the pseudo quantum numbers $N_s = v_1 + v_2 + v_3$ and $N_r = 5v_1 + 3v_2 + 5v_3 + v_4 + v_5$, also accounting for $k = l_4 + l_5$ parity and *e*/*f* symmetry properties. Some 1761 of these lines were excluded from the fit, corresponding either to blended lines, for about 30% of them, or probably to lines perturbed by Coriolis for the remaining ones. The dimensionless standard deviation of the fit is 1.10, and 317 vibration−rotation parameters are determined. These results significantly extend those of a previous report considering levels below only 6750 cm^{-1} [Fayt, A.; et al. *J. Chem. Phys.* **2007**, *126*, 114303]. Unexpected problems are reported when inserting in the global fit the information available on higher-energy polyads, extending from 9300 to 10 120 cm^{-1}. They are tentatively interpreted as resulting from a combination of the relative evolution of the two effective bending frequencies and long-range interpolyad low-order anharmonic resonances. The complete database, made of 18 865 vibration−rotation lines accessing levels up to 10 120 cm^{-1}, is made available as Supporting Information.

1. Introduction

Acetylene is an important, stable, light, and simple molecule. It is therefore an ideal species to produce high-quality spectroscopic data and elaborate quantum models to interpret them. Furthermore, with seven vibrational degrees of freedom, including two doubly degenerate ones, acetylene shows complex intramolecular mechanisms of relevance to understanding the behavior of larger species. Over the years, the ground electronic state of acetylene has been the subject of a number of issues (see reviews in refs 1 and 2). In particular, the interplay between spectroscopy and dynamics stimulated a series of investigations by Field and co-workers.[3−45] Among the breakthroughs resulting from this research performed by the MIT group, the most relevant are the new experimental techniques in the frequency domain to explore the portions of the potential energy surface that are relevant to vibrational intramolecular dynamics, and the development of theoretical approaches to unraveling the resulting spectroscopic data in the time domain. The various inputs contributed significantly to build a global vibrational model in a tetraatomic molecule, exploiting the polyad or cluster structure of the vibrational states. This block diagonal structure emerges from the ratio between the vibrational frequencies, supported by a specific set of anharmonic resonances (see, e.g., ref 25). This model has been supported in the literature by pseudo quantum numbers[46] as well as by a set of rules to predict the number of independent degrees of freedom within the polyad structure.[46−49] This global *vibrational* Hamiltonian has been successfully applied to various acetylene isotopologues in their ground electronic state, over a broad spectral range.[1,2]

More recently, the global Hamiltonian was extended in Brussels to include *rotational* degrees of freedom using the expertise and package of computer programs developed at Louvain-La-Neuve,[50,51] adapted to the acetylene case study. For the first time, the concept of global *vibration−rotation* modeling could be tested over a broad spectral range for a molecule larger than triatomic. The fit of vibration−rotation data over a large energy range to their full instrumental accuracy, ranging from better than 10^{-4} to typically 10^{-3} cm^{-1}, imposed very severe constraints, and the so-called acetylene saga entered a new, significant stage.

The extension toward global vibration−rotation analysis, using *J*-dependent Hamiltonian matrices in a polyad block structure, has so far been successful. All 12 703 published vibration−rotation absorption lines of $^{13}CH^{12}CH$ accessing states up to 6750 cm^{-1},[52] and, later, all 12 137 published vibration−rotation lines in $^{12}C_2H_2$ accessing states up to 8600 cm^{-1},[53] could be accounted for at full instrumental accuracy, meaning within 3σ. For both molecules, the fit excludes a limited number of lines perturbed by Coriolis interactions; however, those are to be included at a later stage of the acetylene saga. The price to pay for this success was the number of parameters, 1 order of magnitude larger compared to the number of pure vibrational fits. However, the number of data simultaneously accounted for increased by more than 2 orders of magnitude and the standard deviation of the fit improved by more than 3 orders of magnitude relative to those for the pure vibrational fits. Thanks to the

† Part of the "Robert W. Field Festschrift".

* To whom correspondence should be addressed. E-mail: M. Herman mherman@ulb.ac.be.
‡ Université Libre de Bruxelles.
§ Université Catholique de Louvain.
|| Università di Bologna.
ARC researcher.
⊥ FRIA researcher.

10.1021/jp904000q CCC: $40.75
Published on Web 07/09/2009

TABLE 1: Survey of the Various Data Sets Used in the Global Vibration−Rotation Fit in $^{13}CH^{12}CH$

	data set			
	#0[a]	A[b]		B
polyads	not detailed	{2,11,1},{3,11,0} {2,12,0},{3,12,1}	{2,13,1},{3,13,0} {3,14,1},{4,14,0}	{3,15,0}
range (cm^{-1})	0−6750	6800−8200	8080−9400	9300−10120
total no. of vib.−rot. lines	12 703	17 225	18 219	18 865
total no. of substates	541	330	468	188
no. of obsd substates	158	64	21	15

[a] Fayt et al., 2007.[52] [b] Data set A is split into two energy ranges for clarity.

reliability of the global vibration−rotation model, such results open a wide range of applications, from astrophysics to dynamics.

The major aim of the present contribution is to test the global vibration−rotation model at even higher energy, up to the 3CH stretching range. For this purpose, we have selected $^{13}CH^{12}CH$ rather than $^{12}C_2H_2$ since the set of data up to about 10 000 cm^{-1} available in the literature is larger in the asymmetric isotopologue, thanks to the absence of *u*/*g* selection rule. Moreover, it is very coherent in terms of calibration, since all transitions above 5000 cm^{-1} arise from the same set of FTIR spectra, recorded in Brussels and analyzed in Bologna.[52,54−57]

The data fitting procedure is presented in section 2, and the results are provided and discussed in sections 3 and 4, respectively, before concluding.

The conventional normal mode numbering in acetylene is used throughout this paper, with 1−5 corresponding to the symmetric CH σ^+ (ν_1) and CC σ^+ (ν_2) stretchings, the antisymmetric CH stretch σ^+ (ν_3), and the *trans*-π (ν_4) and *cis*-π (ν_5) degenerate bendings, respectively. The bends are characterized by the usual bending angular momentum quantum numbers, l_4 and l_5, with $k = l_4 + l_5$. The *e*/*f* parity labels will be used.[58] To avoid confusion in the text, *state* will refer to a vibrational state characterized by the ($\upsilon_1\upsilon_2\upsilon_3\upsilon_4\upsilon_5$) set of quantum numbers, *substate* will indicate an l_i-component of a state identified using either $\upsilon_1\upsilon_2\upsilon_3\upsilon_4\upsilon_5$,$l_4l_5e/f$ or $\upsilon_1\upsilon_2\upsilon_3\upsilon_4^{l_4}\upsilon_5^{l_5}$ values, and *level* will always refer to a specific *J*-value of a state or substate. Polyads will be labeled $\{N_s,N_r,0/1\}$, with $N_s = \upsilon_1 + \upsilon_2 + \upsilon_3$ and $N_r = 5\upsilon_1 + 3\upsilon_2 + 5\upsilon_3 + \upsilon_4 + \upsilon_5$ and 0/1 designating even/odd values of *k*.

2. Data Fitting Procedure

a. Model. As detailed in refs 52 and 54, all states in $^{13}CH^{12}CH$ can be gathered into polyads characterized by the well-known acetylene polyad quantum numbers $\{N_s,N_r\}$, The states within a polyad are connected by a set of anharmonic resonances, namely 11/33, 14/35, 15/34, 1/244, 1/245, 1/255, 3/244, 3/245, 3/255, and 44/55, well determined from spectral analysis.[1,2] The *ij*/*mn* labeling refers to an interaction coupling vibrational states with $\Delta\upsilon_i = \Delta\upsilon_j = \pm 1$ and $\Delta\upsilon_m = \Delta\upsilon_n = \mp 1$. The related $K_{ij/mn}$ and $K'_{ij/mn}$ parameters fulfill the selection rule $\Delta k = 0$ in various possible ways. Polyads include substates with different values of *k*. Indeed, *l*-type vibrational and rotational resonance couples levels in different substates of the same state, with either even or odd *k* values. These are of Σ ($k = 0$), Δ ($k = 2$), Γ ($k = 4$)... or Π ($k = 1$), Φ ($k = 3$)... symmetry, respectively.

The *e* and *f* partition is also applied to build the Hamiltonian in the symmetrized basis as defined in ref 50 for pentaatomic molecules. The resulting vibration−rotation matrices are diagonal in *J*. Each block in the matrix Hamiltonian is characterized not only by the pseudo quantum numbers N_s and N_r but also by the total angular momentum *J*, as well as the symmetry properties *e*/*f*.

The reader is referred to Table 1 in ref 52 for the definition of the various matrix elements and parameters in the model. This includes all anharmonic resonance terms found to be relevant for acetylene up to the highest energy considered so far, i.e., 8600 cm^{-1} in $^{12}C_2H_2$.[53] As in our previous reports,[52−54,59] we select the dominant coefficient in the eigenvector resulting from the Hamiltonian diagonalization at low *J*-values to label states and substates. As a result, in some cases different term values may correspond to the same identification.

Polyads were built up to 11 000 cm^{-1}, and the matrices were set to include all existing states and substates, thus removing the constraints used in our previous papers. Nevertheless, to reduce computing time, the final fits were performed using the limitation $(\upsilon_4 + \upsilon_5)_{max} = 15$ and $k_{max} = 7$, after checking that the results were not affected by the constraints.

b. Data. The literature set of data for $^{13}CH^{12}CH$, up to 6750 cm^{-1}, consisted of 12 703 assigned vibration−rotation line wavenumbers. They were published by the present authors from the detailed analysis of high-resolution absorption spectra.[52,54,55,60−62] We shall refer to this data set as #0. We have now considered 5516 line wavenumbers from the analysis of high-resolution FTIR data, accessing states between 6750 and 9400 cm^{-1}.[57] Together with set #0, they define a new data set labeled A, summarized in Table 1. In the discussion, we shall also consider a third data set, labeled B, also summarized in Table 1. It accounts for the additional 646 published vibration−rotation lines accessing the enegy range between 9300 and 10120 cm^{-1}.[56] Sets A and B cover an additional range of 2650 and 720 cm^{-1}, respectively, above 6750 cm^{-1}. The number of data available severely decreases with increasing energy, while the number of substates (with *e* and *f* parities counted separately) considerably increases, as shown in Table 1.

The full database containing all assigned lines is presented in the Supporting Information. During the present work, a few additional weak bands were identified, and a limited number of lines were reassigned in the spectra previously recorded.[52,54−57] Table 2 provides the results of new band-by-band analyses. The parameters in Table 2 are defined in the following expressions for term values:

$$T(\upsilon, J) = \tilde{\nu}_c + B_\upsilon J(J+1) - D_\upsilon[J(J+1)]^2 + H_\upsilon[J(J+1)]^3 \pm \frac{1}{2}\{q_\upsilon[J(J+1)] + q_\upsilon^J[J(J+1)]^2\} \quad (1)$$

with $\tilde{\nu}_c = G_{\upsilon'}^0 - B_{\upsilon'}k'^2 - D_{\upsilon'}k'^4 - (G_{\upsilon''}^0 - B_{\upsilon''}k''^2 - D_{\upsilon''}k''^4)$ and G_υ^0 the vibrational term value.

For the Δ state, the doubling of the rotational levels was modeled by

$$\pm\frac{1}{4}\{\rho_v J(J+1) + \rho_v^J[J(J+1)]^2\}[J(J+1) - 2] \quad (2)$$

In eqs 1 and 2, the upper signs refer to *e*-parity levels and lower signs to *f*-parity levels.

c. Fitting Procedure. The fitting procedure is identical to the one detailed in our previous global fits,[52,53] based on the package of computer programs developed in Louvain-La-Neuve.[50,51] We used a weighted fitting procedure (weights inversely proportional to the square of the experimental uncertainties) initially accounting for the estimated accuracy (3σ) mentioned by the authors, which is mainly dependent on the technique used and the spectral range investigated. For each set of data, the uncertainty was later reduced in order to agree with the corresponding mean (obsd − calcd) value from the global fit, whenever this value was better than the stated experimental accuracy.

The selection of refined parameters was initially based on the set resulting from the previous investigation up to 6750 cm^{-1}.[52] Later, many additional higher-order parameters were free to vary, under specific constraints.[50] In view of the discussion presented in section 4, it is crucial to stress that numerous tests were performed to avoid constraining the fit to a nonoptimal convergence minimum. For instance, the influence of various sign combinations for the anharmonic resonance parameters was checked carefully. Also, relative intensity features were regularly checked, and detailed analysis of the reduced energy plots was always performed whenever a more complex spectral pattern had to be unraveled. The various checks were applied not only to the newly considered substates but also to those below 6750 cm^{-1}. They were carried out as extensively as possible although, obviously, not exhaustively. No systematic trends were observed from these tests. One can only point out that the convergence of the fit was always slow, requiring many iterations.

Finally, the set of fitted parameters was refined by removing those statistically undetermined one by one, taking care not to affect the dimensionless standard deviation. Also, higher-order coefficients in the model were allowed to vary only if the corresponding lower order was well defined, say within a few percent of its value. In many cases, the quality of the fit was not significantly improved by the refinement of higher-order parameters, and they were then removed in the final stage of the fit.

In sections 3 and 4, we shall successively discuss two of the various fits we have performed in comparison with the previously published one, referred to as "fit 0", considering states up to 6750 cm^{-1}.[52] Fits 1 and 2 include the data sets A and B, as previously defined, respectively. Thus, fit 2 includes all 18 865 available data.

3. Results

The set of 317 parameters listed in Table 3 was obtained from fit 1. As previously defined, the data set includes 18 219 assigned lines involving states up to 9400 cm^{-1}. As in previous similar global fits, these parameters are fully effective, and their selection is not unique. They reproduce 16 458 transitions with a dimensionless standard deviation of 1.10. The statistical survey of the quality of the data set is summarized in Table 4. It is very similar to the results of fit 0 (see Table 4 in ref 52). A total of 1761 lines have been excluded in the final fit (3σ rejection limit). However, as already found in our previous contributions, about 30% of them correspond to blended or very weak lines and were given zero weight. The remaining rejected lines are most likely affected by Coriolis interaction, involving 2/444 or 2/455 mechanisms or other similar combinations of ν_2 and the bends. The Coriolis couplings, perturbing levels by

TABLE 2: Band Centers (ν_c), Vibrational Term Values (G_v), and Rotational Constants in $^{13}CH^{12}CH$ (in cm^{-1}) for Newly Identified Vibration−Rotation Bands[a]

$v_1v_2v_3v_4v_5$, l_4 l_5	transition	ν_c	G_v	B_v	$D_v \times 10^6$	$H_v \times 10^9$	$q_v \times 10^3$ $q_J \times 10^6$ $q_{JJ} \times 10^9$	P, Q, R $\{J_{min},J_{max}\}$	no. fitted/ assigned lines, $\sigma_{lines} \times 10^3$
0 0 1 4 0, 0 0	$\Sigma^+ - \Pi(\nu_4)$	5105.97506(83)	5713.1788	1.148262(21)	10.323(92)			$P_e\{2,14\};R_e\{1,13\}$ $Q_f\{1,15\}$	27/35 2.24
1 0 0 2 1, 2 −1	$^{\Pi}\Pi$ − G.S.	5261.51035(42)	5262.6601	1.149790(12)	4.010(81)	−0.54(15)	−8.798(14) 0.50(12) 1.73(25)	$P_e\{3,15\};R_e\{0,17\}$ $Q_e\{2,31\}$	38/59 1.00
0 1 0 2 3, 0 −1	$^1\Pi$ − G.S.	5307.51711(42)	5308.6671	1.1499848(46)	1.5898(90)		−3.0723(53) 0.320(13)	$P_e\{3,16\};R_e\{0,21\}$ $Q_e\{2,23\}$	46/58 1.29
2 0 0 0 1, 0 1	$\Pi - \Pi(\nu_4)$	6785.81525(12)	7394.1569	1.1379303(15)	1.6365(44)	0.0183(34)	−4.84167(79) 0.1191(12)	$P_e\{2,28\};R_e\{1,29\}$ $P_f\{2,29\};R_f\{1,29\}$	95/113 0.48
1 1 0 0 3, 0 1	$\Pi - \Pi(\nu_4)$	6812.30176(58)	7420.6486	1.1431588(90)	2.842(27)		−10.1586(93) 0.519(37)	$P_e\{5,19\};R_e\{3,17\}$ $P_f\{4,18\};R_f\{2,17\}$	55/61 1.70
0 1 1 3 1, 1 −1	$\Sigma^+ - \Pi(\nu_4)$	7096.97973(35)	7704.1834	1.1421865(85)	−2.162(38)			$P_e\{4,13\}$; $R_e\{4,9\}$ $Q_f\{1,16\}$	17/22 0.75
0 2 1 0 1, 0 1	$\Pi - \Pi(\nu_5)$	7134.20783(21)	7863.5687	1.1328873(39)	1.484(18)	−0.097(22)	−4.5126(20) 0.0321(52)	$P_e\{3,25\};R_e\{1,23\}$ $P_f\{3,23\};R_f\{1,21\}$	59/88 0.55
0 0 2 1 1, 1 −1	$\Sigma^+ - \Pi(\nu_4)$	7171.36394(20)	7778.5676	1.1410421(70)	0.664(54)	2.81(11)		$P_e\{3,14\};R_e\{1,11\}$ $Q_f\{1,18\}$	23/41 0.46
0 0 2 1 1, 1 1	$\Delta - \Pi(\nu_4)$	7185.84976(19)	7797.6155	1.1405121(18)	0.5860(37)		0.003481(11) −0.000722(22)	$P_e\{3,19\};R_e\{1,17\}$ $P_f\{3,23\};R_f\{1,22\}$ $Q_f\{2,27\};Q_e\{2,19\}$	51/121 0.56
1 2 0 0 0, 0 0	Σ^+ − G.S.	7209.19570(38)	7209.1957	1.1308106(56)	1.992(20)	0.203(19)		$P_e\{3,24\};R_e\{1,25\}$	20/47 0.60
0 1 2 0 1, 0 1	Π − G.S.	9122.28331(73)	9123.4184	1.1350824(91)	2.088(23)		−7.005 (11) 0.253(37)	$P_e\{2,19\};R_e\{0,18\}$ $Q_e\{1,22\}$	34/59 1.98

[a] The values of ρ_v and ρ_v^J are listed for Δ states, instead of those of q_v and q_v^J. The standard deviation (1σ) is indicated in parentheses in the unit of the last quoted digit. The assigned lines are listed for each branch. The last column gives the number of lines included in the fit, the number of assigned lines, and the corresponding standard deviation. Rotational lower state constants were constrained to the values from Di Lonardo et al.[61] during the analysis.

TABLE 3: Vibration−Rotation Parameters from the Global Fit of States up to 9400 cm^{-1} for $^{13}CH^{12}CH$ (in cm^{-1})[a]

vibrational diagonal parameters						
om1	3388.74954	0.01533		y4l4l5	0.02119	0.00062	
om2	1950.09472	0.00181		y4l5l5	0.01218	0.00115	
om3	3310.41300	0.01555		y5l4l5	0.04051	0.00132	
om4	604.52472	0.00157		y5l5l5	−0.00180	0.00008	
om5	728.25429	0.00036		z1155	−0.00139	0.00012	
x11	−26.91341	0.01530		z1224	−0.09734	0.00184	
x12	−10.73279	0.00204		z1225	−0.01455	0.00072	
x13	−101.26879	0.00163		z1234	0.09929	0.00358	
x14	−13.46028	0.00608		z1344	0.00880	0.00258	
x15	−11.07921	0.00671		z1444	−0.05644	0.00062	
x22	−7.11847	0.00247		z1445	−0.07828	0.00165	
x23	−4.74361	0.00274		z2223	0.01665	0.00072	
x24	−12.32813	0.00128		z2224	0.02258	0.00049	
x25	−1.54200	0.00072		z2225	0.00843	0.00020	
x33	−27.36795	0.01540		z2234	−0.00805	0.00046	
x34	−9.04427	0.00527		z2244	0.01521	0.00019	
x35	−8.78468	0.00743		z2255	−0.00232	0.00006	
x44	3.15020	0.00199		z2335	−0.01418	0.00269	
x45	−2.37451	0.00135		z2355	−0.02150	0.00089	
x55	−2.42886	0.00034		z2444	0.00405	0.00016	
xl4l4	0.64411	0.00151		z2445	−0.00487	0.00033	
xl4l5	6.54541	0.00095		z2455	0.00791	0.00025	
xl5l5	3.54486	0.00043		z2555	0.00164	0.00002	
y112	0.07739	0.00135		z3344	0.09597	0.00387	
y115	0.27041	0.00652		z3345	0.07119	0.00185	
y122	−0.18821	0.00090		z3355	−0.04373	0.00066	
y123	−0.17778	0.00225		z3444	0.01344	0.00065	
y124	0.11696	0.00229		z3445	0.05290	0.00104	
y125	0.14397	0.00110		z3555	0.04880	0.00105	
y134	0.04806	0.00733		z4444	−0.00499	0.00003	
y135	−0.36834	0.00843		z4445	0.00606	0.00048	
y144	0.16217	0.00263		z4455	0.01831	0.00019	
y145	−0.08274	0.00381		z4555	−0.00460	0.00014	
y155	0.04898	0.00046		z5555	−0.00018	0.00000	
y222	−0.01922	0.00070		z11l5l5	−0.00283	0.00009	
y223	−0.10232	0.00255		z12l4l4	0.00348	0.00091	
y224	−0.30081	0.00154		z13l4l4	−0.02172	0.00302	
y225	−0.09948	0.00092		z13l5l5	0.14976	0.00551	
y233	−0.37039	0.00133		z14l4l4	0.02240	0.00098	
y234	−0.01202	0.00169		z14l4l5	−0.04570	0.00099	
y235	0.18827	0.00207		z14l5l5	−0.01514	0.00043	
y244	0.37863	0.00090		z15l4l4	0.10634	0.00254	
y245	−0.08180	0.00073		z24l4l4	−0.00263	0.00030	
y255	−0.05269	0.00022		z24l4l5	−0.00558	0.00037	
y334	−0.56199	0.00461		z24l5l5	−0.00914	0.00032	
y335	−0.12475	0.00636		z25l4l4	0.01992	0.00069	
y344	−0.17619	0.00486		z33l4l4	0.04017	0.00103	
y345	0.03417	0.00337		z33l4l5	−0.03077	0.00109	
y355	−0.07789	0.00339		z33l5l5	0.00749	0.00047	
y444	0.00879	0.00070		z34l4l4	−0.03650	0.00035	
y445	0.08244	0.00146		z34l4l5	0.01974	0.00076	
y455	0.04969	0.00039		z34l5l5	0.03966	0.00153	
y555	0.01033	0.00006		z35l4l4	−0.05073	0.00103	
y1l4l4	−0.19356	0.00349		z35l4l5	−0.02209	0.00123	
y1l4l5	−0.10557	0.00222		z44l4l4	0.00541	0.00014	
y1l5l5	−0.06612	0.00044		z44l4l5	0.00707	0.00023	
y2l4l4	−0.15539	0.00097		z44l5l5	−0.01192	0.00035	
y2l4l5	0.00782	0.00063		z45l4l4	−0.01398	0.00017	
y2l5l5	0.00861	0.00026		z45l5l5	−0.00291	0.00025	
y3l4l4	0.03023	0.00067		z55l4l5	−0.01029	0.00046	
y3l4l5	−0.02880	0.00077		zl4444	−0.00080	0.00005	
y3l5l5	−0.03061	0.00104		zl5555	−0.00015	0.00000	
y4l4l4	0.02614	0.00095					
rotational diagonal parameters							
B0	1148.46119	0.00022	E-03	eps245	0.28428	0.01161	E-05
alpha1	6.41409	0.00343	E-03	eps334	−0.44555	0.07637	E-05
alpha2	5.97540	0.00035	E-03	eps344	0.24776	0.02848	E-05
alpha3	5.64452	0.00343	E-03	eps444	0.08651	0.00279	E-05
alpha4	−1.18794	0.00014	E-03	eps455	−0.17541	0.00310	E-05
alpha5	−2.08073	0.00008	E-03	eps2l44	−0.13665	0.02297	E-05
gam11	−10.23134	0.33453	E-05	eps2l45	−0.41985	0.01375	E-05
gam12	5.81168	0.04482	E-05	eps2l55	−0.38929	0.00773	E-05
gam13	−19.66354	0.05431	E-05	eps3l44	−0.35778	0.03659	E-05
gam14	8.95215	0.11405	E-05	eps3l45	0.31561	0.03215	E-05
gam15	2.88604	0.02358	E-05	eps3l55	0.08584	0.02187	E-05
gam22	−2.13944	0.03224	E-05	eps4l45	0.28731	0.00646	E-05
gam23	6.36153	0.07928	E-05	eps5l44	−0.04767	0.00453	E-05
gam24	−6.78445	0.03551	E-05	eps5l45	−0.66733	0.00328	E-05
gam25	−5.30114	0.01785	E-05	eps5l55	−0.17546	0.00214	E-05
gam33	7.07332	0.33563	E-05	D0	1.55765	0.00022	E-06
gam34	6.26365	0.09795	E-05	beta1	−1.83977	0.03171	E-08

TABLE 3: Continued

gam35	2.66422	0.04781	E-05	beta2	0.26776	0.01151	E-08
gam44	−0.39014	0.01283	E-05	beta3	−0.69031	0.04767	E-08
gam45	−2.10500	0.00928	E-05	beta4	2.96225	0.01291	E-08
gam55	2.29848	0.00424	E-05	beta5	2.34789	0.00346	E-08
gl4l4	−6.11183	0.00730	E-05	beta11	38.31289	2.44580	E-10
				rotational diagonal parameters			
gl4l5	−21.69560	0.01020	E-05	beta23	−44.29119	3.28833	E-10
gl5l5	−10.63622	0.00723	E-05	beta24	−14.22060	1.43542	E-10
eps114	0.84476	0.06022	E-05	beta33	−43.66752	3.96398	E-10
eps123	0.43817	0.10594	E-05	beta34	18.56706	3.09929	E-10
eps125	−0.44239	0.03063	E-05	beta35	−33.42888	2.95836	E-10
eps134	1.37135	0.09296	E-05	beta44	−3.49241	0.56880	E-10
eps135	1.11529	0.08624	E-05	beta45	−2.91565	0.26385	E-10
eps144	0.70835	0.03958	E-05	beta55	1.80892	0.15291	E-10
eps223	0.56753	0.04179	E-05	betal44	7.52865	1.48459	E-10
eps224	0.48441	0.02038	E-05	betal45	−46.21569	0.37485	E-10
eps225	0.30715	0.01527	E-05	betal55	−13.16146	0.27430	E-10
eps244	−0.16056	0.01817	E-05	H0	1.48805	0.06242	E-12
				rotational l-type resonances			
q4	−5.02094	0.00008	E-03	q5v3	−0.00530	0.00055	E-03
q4v1	−0.01282	0.00096	E-03	q5v4	−0.10890	0.00029	E-03
q4v2	−0.02442	0.00043	E-03	q5v5	−0.04143	0.00009	E-03
q4v3	−0.04159	0.00139	E-03	q5v13	2.99336	0.16570	E-05
q4v4	0.00966	0.00008	E-03	q5v24	−0.74460	0.01833	E-05
q4v5	−0.06461	0.00009	E-03	q5v25	0.24230	0.00660	E-05
q4v13	2.48257	0.10754	E-05	q5v44	0.66451	0.01871	E-05
q4v14	2.58292	0.08063	E-05	q5v55	−0.04860	0.00356	E-05
q4v22	0.29568	0.03380	E-05	q5J	3.59768	0.00923	E-08
q4v23	−0.74082	0.04041	E-05	q5Jv1	0.10609	0.02288	E-08
q4v24	0.51898	0.04176	E-05	q5Jv3	0.67789	0.04569	E-08
q4v25	0.27426	0.02674	E-05	q5Jv4	0.35339	0.00624	E-08
q4v33	2.29278	0.13123	E-05	q5Jv5	0.10347	0.00439	E-08
q4v34	0.47633	0.04454	E-05	q5JJ	−0.28264	0.03044	E-12
q4v45	−0.18249	0.01190	E-05	q445	−0.19757	0.00670	E-05
q4J	3.66077	0.01384	E-08	u44	−0.13940	0.00992	E-08
q4Jv2	0.11993	0.03134	E-08	u45	−0.18413	0.00495	E-08
q4Jv5	0.21320	0.00761	E-08	u45v4	4.20176	0.49270	E-10
q4JJ	−0.40870	0.06278	E-12	u45v5	−4.51928	0.64416	E-10
q5	−4.48229	0.00007	E-03	u45J	0.00236	0.00031	E-10
q5v1	−0.04445	0.00034	E-03	u55	−0.10326	0.00115	E-08
q5v2	0.00304	0.00009	E-03				
				vibrational l-type resonances			
r45	−6.20167	0.00001		r45v34	8.11823	0.15069	E-02
r45v1	0.02626	0.00357		r45v45	−2.06996	0.03079	E-02
r45v2	0.10262	0.00094		r45l44	0.13334	0.00540	E-02
r45v3	0.27377	0.00282		r45l55	−0.17995	0.00726	E-02
r45v4	0.02889	0.00091		r45J	18.98397	0.00502	E-05
r45v5	0.07143	0.00091		r45Jv3	−0.72131	0.04618	E-05
r45v11	−5.90068	0.21061	E-02	r45Jv4	−0.47182	0.00703	E-05
r45v12	−2.07533	0.14630	E-02	r45Jv5	0.74544	0.00480	E-05
r45v14	−1.95466	0.10010	E-02	r45JJ	−35.98604	0.43619	E-10
r45v15	−5.59851	0.09033	E-02	r4455	0.00357	0.00008	
				anharmonic resonances			
k1244	12.06135	0.03034		o3245	4.88421	0.11841	E-05
k1244v1	0.79264	0.03361		k1133	−109.27131	0.09007	
k1244v4	0.36011	0.01386		k1133v4	1.27204	0.01380	
k1244J	−24.98297	1.02159	E-05	k1133v5	1.46359	0.03685	
o1244	5.26222	0.63169	E-05	k1133J	−63.84169	1.92258	E-05
k1255	7.22659	0.00481		k1435	31.99420	0.02775	
k1255v2	−0.14978	0.00223		k1435v1	2.12061	0.04174	
k1255v4	−0.15239	0.00322		k1435v2	−1.62175	0.01042	
k1255J	−7.22877	0.10754	E-05	k1435v3	−2.90861	0.04064	
o1255	−3.24113	0.04861	E-05	k1435v4	−1.08957	0.01416	
k1245	4.98335	0.02150		k1435v5	−0.25105	0.00449	
k1245v4	0.30166	0.00961		k1435J	−34.75427	0.36357	E-05
k1245v5	0.54755	0.01400		o1435	−7.57784	0.09980	E-05
k1245J	−19.26558	0.69405		k1534	34.21607	0.07458	
k3244	4.10691	0.02678		k1534v1	−0.91716	0.08288	
k3244v1	0.92616	0.03535		k1534v2	−1.19876	0.03594	
k3244v4	0.06742	0.01295		k1534v3	0.67849	0.06319	
k3244J	−47.70422	1.55359		k1534v4	−1.24125	0.02366	
k3255	0.56004	0.02406		k1534J	−48.69434	1.02732	E-05
k3255J	−67.12384	1.40302	E-05	o1534	−12.38128	0.38129	E-05
o3255	2.51354	0.69750	E-05	k4455	−9.31750	0.01185	
k3245	−17.05777	0.01390		k4455v1	0.84919	0.01967	
k3245v1	−0.83464	0.03307		k4455v2	0.25408	0.01174	
k3245v2	0.43239	0.01193		k4455v3	−0.97054	0.02926	
k3245v3	0.26174	0.02379		k4455v4	0.84801	0.00649	
k3245v4	0.26340	0.00358		k4455v5	0.01456	0.00398	
k3245v5	0.23279	0.00187		k4455J	14.63627	0.14436	E-05
k3245v44	−0.01512	0.00158		kp4455	3.97485	0.02194	
k3245v45	−0.07304	0.00228		kp4455v2	0.12691	0.00678	
k3245J	22.67018	0.17386	E-05	kp4455v4	0.34794	0.00434	
k3245JJ	−92.51342	6.76410	E-10				

[a] The standard deviation (1σ) is indicated. The parameters are labeled in agreement with the model defined in the text. They are provided as directly printed by the computer package of programs used.

TABLE 4: Statistical Survey of the Quality of the Vibration−Rotation Data Set in $^{13}CH^{12}CH$ and of the Deviation from the Global Fit

exp acc	$\leq 6 \times 10^{-4}$ cm^{-1}	$\leq 10^{-3}$ cm^{-1}	$\leq 10^{-2}$ cm^{-1}	$\leq 5 \times 10^{-2}$ cm^{-1}	total
lines fitted	6131	5692	4588	47	16458
fraction, %	37.2	34.6	27.9	0.3	100

less than 0.01 cm^{-1}, will tentatively be included in the global model at a later stage of the acetylene saga.

The parameters listed in Table 3 compare well with those of fit 0 previously published,[52] thus also fulfilling $x-K$ relations.[54]

As a typical example of the quality of the results, observed and simulated spectra in the 6500 cm^{-1} range are illustrated in Figure 1. Figures 2 and 3 detail the perturbation schemes affecting the zero-order (10110,10) Π substate at 7124.37 cm^{-1}. This substate is observed through both cold and hot bands. The latter, involving ν_4 as the lower state, is shown in Figure 1. Only three zero-order vibrational transition moments, $\mathbf{R}_v$, were inserted in the simulation presented in Figure 1a, with relative values of $|R_v^{10100}| = 1.0$, $|R_v^{00200}| = 0.2$, and $|R_v^{20000}| = 0.1$. All intensity borrowings derive from the composition of the eigenvectors resulting from the energy matrix diagonalization. Hot bands are also simulated from the same parameters, using the Boltzmann factor to adapt the intensity. For completeness, one should mention that the weaker sub-bands in the range of Figure 1, not relevant to the present discussion, are not simulated because they would require additional intensity parameters. A portion of the spectrum is highlighted in Figure 1b. The upper J-value in the R branches of three relevant sub-bands are indicated. It is interesting to notice that the spacing between e (labeled +) and f (labeled •) lines in the $\nu_1 + \nu_3 + \nu_4 \leftarrow \nu_4$ sub-band increases on going from $J' = 15$ to 16. The reduced energy graph in Figure 2a shows that the e parity levels of (10110,10) present two avoided crossings, one with the (01121,21) Φ_e substate around $J' = 15$, and one with the (01121,01) Π_e substate around $J' = 27$. Both perturbers are highly mixed with each other by rotational l-type resonance terms. Similar interaction is observed between the f-parity levels, with only one major avoided crossing around $J' = 25$. Figure 2b details the situation around $J' = 15$. Since the f-components are not affected around $J' = 15$ (see black dots in Figure 2a), the e/f spacing increases only as a result of the avoided crossing for the e levels.

In addition, zero-order forbidden rotational branches are observed for the (01121,21) $\Phi_{e,f}$ substates, in both cold and hot bands. Forbidden R branch lines from the $\Delta k = 2$ selection rule in the (01121,21) ← (00010,10) $\Phi_e - \Pi_f$ band are indicated in Figure 1b (red □). The J-dependence of the coefficients of the eigenvector of the (01121,21) Φ_e substate and the corresponding avoided crossing are illustrated in Figure 3. The labels for the relevant zero-order substates are the same for Figures 1−3. The analysis of this range could be finalized only using the present global results.

4. Discussion

A detailed comparison of the parameters of fit 1 presented in Table 3 with those of fit 0 previously published demonstrates that, while all lower-order parameters are very similar, the sizes of some high-order anharmonic resonance ones is different. In particular, this is the case for several K_{ijkl,v_m} parameters. Their definition is recalled in eqs 3 and 4 for the 3/245 resonance, selected as an example.

$$\langle v_1,\ v_2,\ v_3,\ v_4^{l_4},\ v_5^{l_5}|\tilde{H}|v_1,\ v_2 - 1,\ v_3 + 1,\ (v_4 - 1)^{l_4 \pm 1},\ (v_5 - 1)^{l_5 \mp 1}\rangle = -{}^1/_8 K_{3/245}[v_2(v_3 + 1)(v_4 \mp l_4)(v_5 \pm l_5)]^{1/2} \quad (3)$$

$$K_{3/245} = K^0_{3/245} + \sum_i K_{3/245,i}(v_i - \delta_{i2} - \delta_{i4} - \delta_{i5}) + \sum_i K_{3/245,ij}(v_i - \delta_{i2} - \delta_{i4} - \delta_{i5})(v_j - \delta_{j2} - \delta_{j4} - \delta_{j5}) + K_{3/245,J}[J(J+1) - k^2] + K_{3/245,JJ}[J(J+1) - k^2]^2 \quad (4)$$

with δ_{ij} the usual Kronecker symbol.

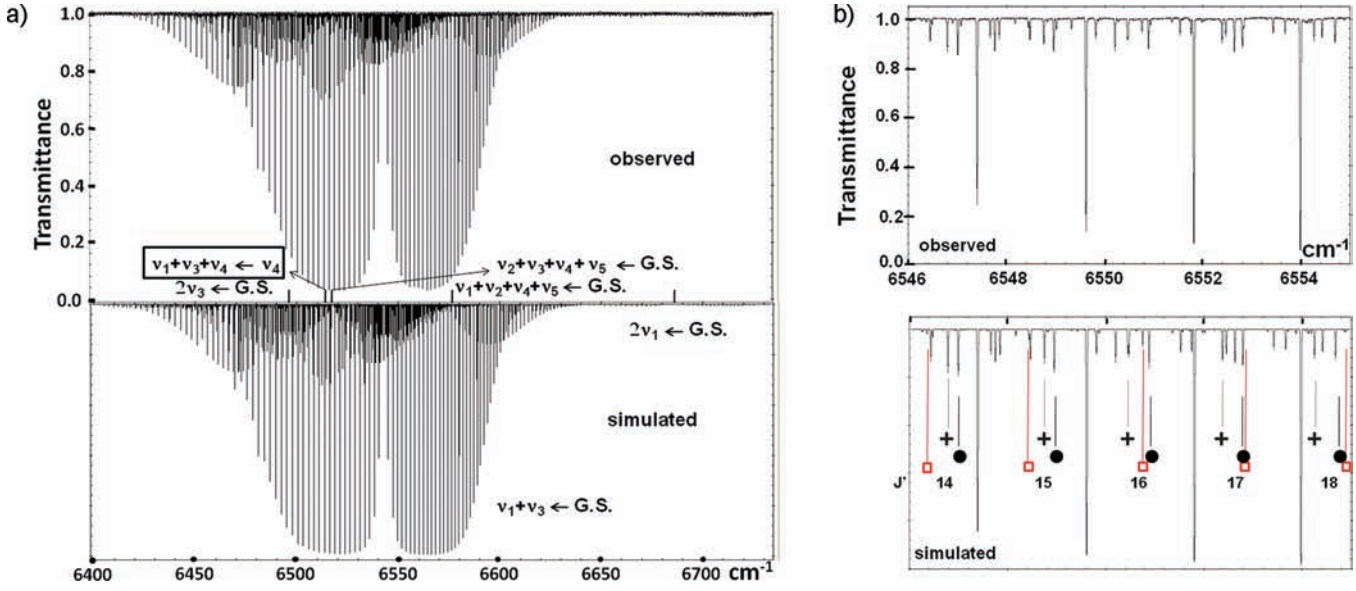

Figure 1. (a) FT transmittance spectrum of $^{13}CH^{12}CH$ between 6400 and 6760 cm^{-1}. The main bands are identified and assigned. Experimental conditions: cell pressure 0.088 hPa, absorption path length 55.1 m. (b) Expansion of a portion of the transmittance spectrum, with some relevant lines, all from R branches, assigned (see text). Observed and simulated spectra are presented.

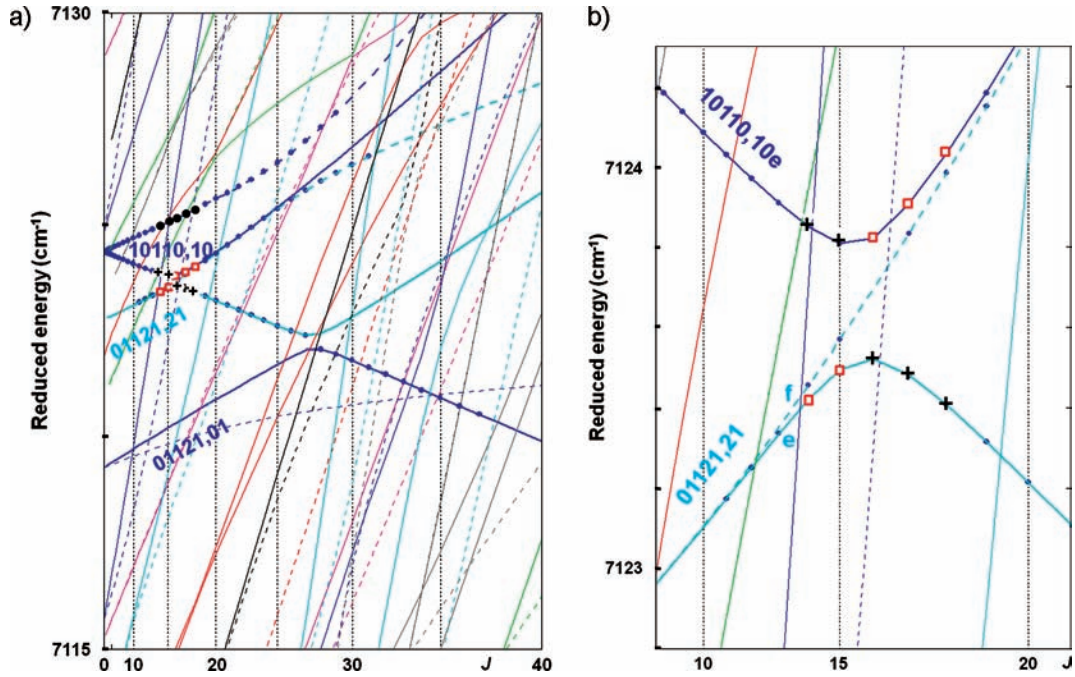

Figure 2. Reduced vibration−rotation energies as a function of $J(J+1)$ for the substates of $^{13}CH^{12}CH$ between 7115 and 7130 cm^{-1}. The reduced energy (in cm^{-1}) corresponds to $E_{vr} - B_0J(J+1) + D_0J^2(J+1)^2$, with $B_0 = 1.137760$ cm^{-1} and $D_0 = 1.5567 \times 10^{-6}$ cm^{-1}. The relevant substates are identified in terms of ($v_1v_2v_3v_4v_5$,l_4l_5, *e*/*f*). The symbol *x* replacing *e*/*f* means that both components are quasi degenerate at J_{min}. Components of *e* (*f*) symmetry are plotted in full (dotted) lines. The color code associated with the relevant states is dark and light blue for Π and Φ zero-order symmetries, respectively. Dots (•) indicate sublevels reached by vibration−rotation transitions assigned in the experimental spectrum and fitted. (a) The full range of interest and (b) detail of one of the avoided crossings. Dots are replaced by other signs for those levels around $J' = 15$: (01121,21) □, (10110,10) +, see text.

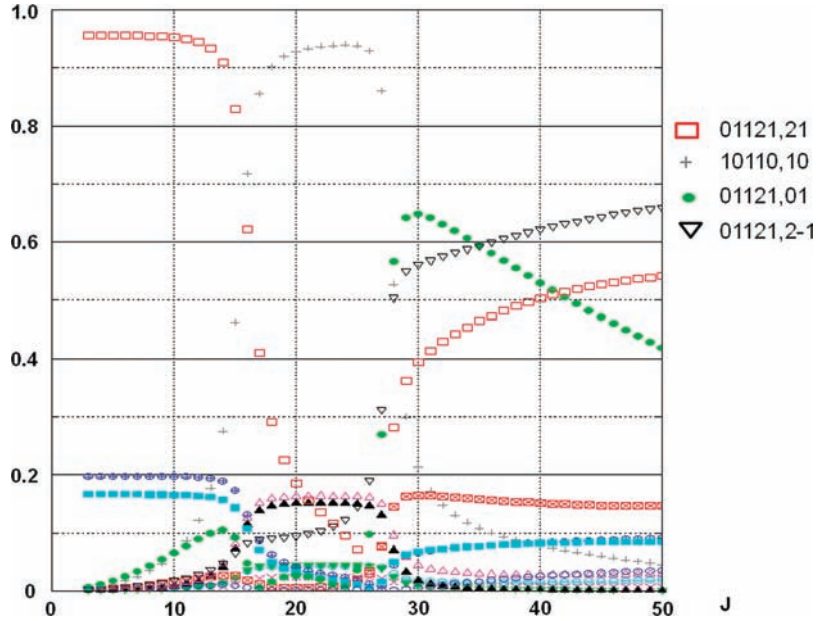

Figure 3. *J*-dependence of the coefficients of the eigenvectors of the set of levels that, at low *J*-values, correspond to the (01121,21) Φ_e substate of $^{13}CH^{12}CH$ (light blue). The main zero-order substates involved in the coupling mechanisms discussed in the text are assigned.

The inclusion of the higher-energy polyads in fit 2 dramatically increases the problem. In some cases, the high-order parameters are now more than half of the value of the corresponding lower-order ones, as illustrated in Table 5. Those additional, problematic parameters proved to be essential to achieve an acceptable standard deviation within the 3σ rejection limit.

Given these anomalies with fit 2, we restricted the final results to fit 1, in the previous section. The results of fit 2, which contain the full set of substates, 319 parameters determined and a dimensionless standard deviation of 2.62, are only provided in the Supporting Information. The parameters from fit 1 are repeated in the Supporting Information, for completeness.

The observed behavior could arise from the very large number of parameters and associated degrees of freedom in the fit. Nonoptimal numerical convergence could have resulted from a fit biased by some inadequate procedure. However, the tests mentioned in section 2 to avoid convergence problems, and the high quality of fit 1, which is comparable to those previously achieved in acetylene, including fit 0, seem to support the

TABLE 5: Illustration of the Trends in the Evolution of Selected Higher Order Resonance Parameters for the Global Model in $^{13}CH^{12}CH$, for Successive Fits[a]

	0[b]	1	2
$K_{1/244,v_3}$	not fitted	not fitted	45.7
$K_{1/245,v_1}$	not fitted	not fitted	−11.5
$K_{1/245,v_3}$	not fitted	not fitted	19.3
$K_{3/244,v_1}$	not fitted	22.5	32.3
$K_{3/244,v_2}$	not fitted	not fitted	14.6
$K_{3/244,v_3}$	not fitted	not fitted	30.0
$K_{3/244,v_5}$	not fitted	not fitted	−74.1
$K_{3/245,v_1}$	not fitted	4.9	−14.6
$K_{11/33,v_4}$	not fitted	−1.2	6.4
$K_{11/33,v_5}$	not fitted	−1.3	−10.7
$K_{14/35,v_3}$	not fitted	−9.1	−13.2

[a] For the definition of the parameters and of the fits, see text. The numbers correspond to the ratio between the value of the parameter and that of the corresponding zero-order resonance parameter, in %. [b] Fayt et al., 2007.[52]

procedure and to rule out problems of pure numerical nature. More physical reasons are likely to be responsible for the failure of the model.

One could invoke the isomerization to vinylidene,[63,64] also investigated by Field's group at MIT.[10,11,34,41] The global model has no way to account for the new states and new interaction mechanisms that would result from the isomerization process. However, though not very precisely characterized yet, the barrier for isomerization is expected to occur in the early visible range, i.e., far away from the spectral region presently investigated. It is therefore unlikely to be responsible for the trends presently reported.

Another mechanism is to be mentioned. The vibrational parameters of the *trans* ($\tilde{\omega}_4 = 604.5$ cm^{-1}, $x_{44} = 3.15$ cm^{-1}) and *cis* ($\tilde{\omega}_5 = 728.3$ cm^{-1}, $x_{55} = -2.43$ cm^{-1}) bending vibrations are such that the two vibrational term values are close around $v_b = 11$ (with $b = 4$ or 5), i.e., around 7500 cm^{-1}. Although the global effective Hamiltonian is, in principle, able to deal with this situation,[28,31] it could represent the onset of interesting vibrational behavior and be responsible for the slow convergence in the fitting procedure. Similar problems are mentioned in the *ab initio* literature and attributed to the evolution of the *trans* bending vibration.[65−67]

Finally, one should examine the role of interpolyad resonances. Recent results from Perevalov and co-workers concerning triatomic species demonstrate that interpolyad anharmonic resonances occur in CO_2[68−70] and probably in N_2O.[71] They connect substates in two successive polyads and cause perturbations affecting specific levels. Such local effects could also arise in the present case. For instance, polyad {3,15,0}, which includes all levels in set B (3 CH range), extends from 9308 to 10 121 cm^{-1}. It is partly overlapped by polyad {4,16,0}, whose substates cover the range between 9956 and 10 567 cm^{-1}. Substates (30000) and (22000) belong to these polyads, respectively. They are connected by the 1/22 resonance, which is not included in the global model. These two substates are separated by about 570 cm^{-1}. Using the cubic anharmonic force constants reported by Martin et al.,[66] the expression in eq 6 from Law and Duncan[72] for the resonance parameter, and the harmonic wavenumbers from Table 3, we calculated $K_{1/22} \approx -70$ cm^{-1}. The result is that the two levels are pushed apart by about 13 cm^{-1}. Though not predicted in the *ab initio* literature,[65−67] the value of $K_{1/22}$ looks reasonable for a first-order anharmonic resonance. However, as pointed out in ref 72, the discrepancy between experimental and calculated $K_{1/22}$ can be rather large. Nevertheless, one can expect the 1/22 resonance to show up and affect not only the states just selected but others as well, such as (10000) and (02000), or (12031) and (04031). The effect will vary because of the different energy separation (about 510 and 450 cm^{-1}, respectively) and the v-dependence of the coupling matrix elements. The same probably applies to other relevant interpolyad low-order interactions, such as 3/22 or 2/44. Given the network of interactions within a polyad, local effects can thus be expected if the interaction extends to substates in each polyad that are close in energy. More likely, *long-range* anharmonic interactions spread over many substates may result between the two polyads, and those are likely to explain the observed behavior. These effects were most likely previously absorbed by the effective Hamiltonian, but, since they do not regularly scale with energy, their contribution is not fully accounted for, thus causing the reported problems.

At the present stage, we can thus suggest two possible contributions to the fitting problems. Slow convergence might have been induced by the evolution of v_4 with respect to v_5, while long-range interpolyad low-order resonances could cause significant failures in the global vibration−rotation model at the required level of accuracy.

5. Conclusion

All known vibration−rotation absorption lines of $^{13}CH^{12}CH$ accessing levels up to 10 120 cm^{-1}, including some transitions assigned during the present work, were gathered. They were fitted simultaneously to J-dependent Hamiltonian matrices exploiting the well-known vibrational polyad or cluster block-diagonalization, in terms of the pseudo quantum numbers $N_s = v_1 + v_2 + v_3$ and $N_r = 5v_1 + 3v_2 + 5v_3 + v_4 + v_5$, and accounting also for k-parity and *e/f* symmetry properties. We have succeeded in fitting 16 458 vibration−rotation lines, within the 9400 cm^{-1} energy limit, with a dimensionless standard deviation of 1.10, leading to the determination of 317 vibration−rotation parameters. The other 1761 lines in the literature within this energy limit are likely to be either blended or perturbed by Coriolis coupling, not yet included in the global model. The remaining 646 higher-energy lines could be accounted for only at the expense of the unexpectedly large evolution of higher-order anharmonic resonance parameters. General insight into this problem has been suggested, in terms of the interaction between highly excited bending states and of first-order interpolyad anharmonic resonances. It will be interesting to investigate whether this problem is also encountered in $^{12}C_2H_2$ as well as to stimulate new *ab initio* calculations to characterize all anharmonic resonances in the molecule.

The present results significantly extend those in the literature and, at the same time, evidence some failure in the global model. They explain numerous complicated perturbations in the spectrum and permit a number of investigations to be undertaken, of dynamical and astrophysical nature, within the broad energy range presently investigated.

Acknowledgment. We are indebted to Dr. J. Vander Auwera (ULB) for recording the spectra presently used. S.R. and B.A. thank ARC and FRIA, respectively, for financial support. This work was sponsored, in Italy, by the Università di Bologna and MIUR (PRIN "Trasferimenti di energia e di carica: dalle collisioni ai processi dissipativi") and, in Belgium, by the Fonds National de la Recherche Scientifique (FNRS, contracts FRFC and IISN) and the "Action de Recherches Concertées de la Communauté française de Belgique". It is performed within the "LEA HiRes" collaboration between ULB and UCL.

Supporting Information Available: Parameters resulting from fits 1 and 2 in $^{13}CH^{12}CH$; summary of vibration−rotation bands in the $^{13}CH^{12}CH$ database used for the global fit; and table of the vibration−rotation lines used in the global vibration−rotation fitting in $^{13}CH^{12}CH$. This material is available free of charge via the Internet at http://pubs.acs.org.

References and Notes

(1) Herman, M. *Mol. Phys.* **2007**, *105*, 2217.
(2) Herman, M. In *Handbook of High Resolution Spectroscopy*; Quack, M. Merkt, F., Eds.; Wiley: New York, 2009, in press.
(3) Abramson, E.; Field, R. W.; Imre, D.; Innes, K. K.; Kinsey, J. L. *J. Chem. Phys.* **1984**, *80*, 2298.
(4) Abramson, E.; Field, R. W.; Imre, D.; Innes, K. K.; Kinsey, J. L. *J. Chem. Phys.* **1985**, *83*, 453.
(5) Sundberg, R. L.; Abramson, E.; Kinsey, J. L.; Field, R. W. *J. Chem. Phys.* **1985**, *83*, 466.
(6) Pique, J. P.; Chen, Y.; Field, R. W.; Kinsey, J. L. *Phys. Rev. Lett.* **1987**, *58*, 475.
(7) Pique, J. P.; Lombardi, M.; Chen, Y.; Field, R. W.; Kinsey, J. L. *Ber. Bunsenges. Phys. Chem.* **1988**, *92*, 422.
(8) Pique, J. P.; Chen, Y.; Field, R. W.; Kinsey, J. L. *J. Phys., Colloque* **1987**, *C7*, C7.
(9) Pique, J. P.; Engel, Y. M.; Levine, R. D.; Chen, Y.; Field, R. W.; Kinsey, J. L. *J. Chem. Phys.* **1988**, *88*, 5972.
(10) Chen, Y.; Jonas, D. M.; Hamilton, C. E.; Green, P. G.; Kinsey, J. L.; Field, R. W. *Ber. Bunsenges. Phys. Chem.* **1988**, *92*, 329.
(11) Chen, Y.; Jonas, D. M.; Kinsey, J. L.; Field, R. W. *J. Chem. Phys.* **1989**, *91*, 3976.
(12) Green, P. G.; Kinsey, J. L.; Field, R. W. *J. Chem. Phys.* **1989**, *91*, 5160.
(13) Chen, Y.; Halle, S.; Jonas, D. M.; Kinsey, J. L.; Field, R. W. *J. Opt. Soc. Am. B: Opt. Phys.* **1990**, *7*, 1805.
(14) Yamanouchi, K.; Ikeda, N.; Tsuchiya, S.; Jonas, D. M.; Lundberg, J. K.; Adamson, G. W.; Field, R. W. *J. Chem. Phys.* **1991**, *95*, 6330.
(15) Jonas, D. M.; Solina, S. A. B.; Rajaram, B.; Silbey, R. J.; Field, R. W.; Yamanouchi, K.; Tsuchiya, S. *J. Chem. Phys.* **1992**, *97*, 2813.
(16) Pique, J. P.; Chen, Y.; Field, R. W.; Kinsey, J. L. *Phys. Rev. Lett.* **1992**, *69*, 2019.
(17) Lundberg, J. K.; Jonas, D. M.; Chen, Y.; Rajaram, B.; Field, R. W. *J. Chem. Phys.* **1992**, *97*, 7180.
(18) Lundberg, J. K.; Field, R. W.; Sherrill, C. D.; Seidl, E. T.; Xie, Y.; Schaefer, H. F., III. *J. Chem. Phys.* **1993**, *98*, 8384.
(19) Jonas, D. M.; Solina, S. A. B.; Rajaram, B.; Cohen, S. J.; Silbey, R. J.; Field, R. W.; Yamanouchi, K.; Tsuchiya, S. *J. Chem. Phys.* **1993**, *99*, 7350.
(20) Yamanouchi, K.; Miyawaki, J.; Tsuchiya, S.; Jonas, D. M.; Field, R. W. *Laser Chem.* **1994**, *14*, 183.
(21) Solina, S. A. B.; O'Brien, J. P.; Field, R. W.; Polik, W. F. *Ber. Bunsenges. Phys. Chem.* **1995**, *99*, 555.
(22) Coy, S. L.; Chasman, D.; Field, R. W. In *Molecular Dynamics and Spectroscopy by Stimulated Emission Pumping*; Dai, H.-L., Field, R. W., Eds.; Advanced Series in Physical Chemistry *4*; World Scientific: Singapore, 1995; p 891.
(23) Yamanouchi, K.; Field, R. W. *Laser Chem.* **1995**, *16*, 31.
(24) Solina, S. A. B.; O'Brien, J. P.; Field, R. W.; Polik, W. F. *J. Phys. Chem.* **1996**, *100*, 7797.
(25) Abbouti Temsamani, M.; Herman, M.; Solina, S. A. B.; O'Brien, J. P.; Field, R. W. *J. Chem. Phys.* **1996**, *105*, 11357.
(26) Field, R. W.; O'Brien, J. P.; Jacobson, M. P.; SolinaS. A. B.; Polik, W. F.; Ishikawa, H. In *Chemical Reactions and Their Control on the Femtosecond Time Scale*; Gaspard, P., Burghardt, I., Eds.; Advances in Chemical Physics *101*; Wiley: New York, 1997; p 463.
(27) O'Brien, J. P.; Jacobson, M. P.; Sokol, J. J.; Coy, S. L.; Field, R. W. *J. Chem. Phys.* **1998**, *108*, 7100.
(28) Jacobson, M. P.; O'Brien, J. P.; Silbey, R. J.; Field, R. W. *J. Chem. Phys.* **1998**, *109*, 121.
(29) Jacobson, M. P.; O'Brien, J. P.; Field, R. W. *J. Chem. Phys.* **1998**, *109*, 3831.
(30) Jacobson, M. P.; Silbey, R. J.; Field, R. W. *J. Chem. Phys.* **1999**, *110*, 845.
(31) Jacobson, M. P.; Jung, C.; Taylor, H. S.; Field, R. W. *J. Chem. Phys.* **1999**, *111*, 600.
(32) Moss, D. B.; Duan, Z.; Jacobson, M. P.; O'Brien, J. P.; Field, R. W. *J. Mol. Spectrosc.* **2000**, *199*, 265.
(33) Jacobson, M. P.; Field, R. W. *Chem. Phys. Lett.* **2000**, *320*, 553.
(34) Jacobson, M. P.; Field, R. W. *J. Phys Chem. A* **2000**, *104*, 3073.
(35) Altunata, S.; Field, R. W. *J. Chem. Phys.* **2000**, *113*, 6640.
(36) Srivastava, H. K.; Conjusteau, A.; Mabuchi, H.; Callegari, A.; Lehmann, K. K.; Scoles, G.; Silva, M. L.; Field, R. W. *J. Chem. Phys.* **2000**, *113*, 7376.
(37) Altunata, S.; Field, R. W. *J. Chem. Phys.* **2001**, *114*, 6557.
(38) Hoshina, K.; Iwasaki, A.; Yamanouchi, K.; Jacobson, M. P.; Field, R. W. *J. Chem. Phys.* **2001**, *114*, 7424.
(39) Silva, M. L.; Jacobson, M. P.; Duan, Z.; Field, R. W. *J. Mol. Struct.* **2001**, *565*−*566*, 87.
(40) Silva, M. L.; Jacobson, M. P.; Duan, Z.; Field, R. W. *J. Chem. Phys.* **2002**, *116*, 7939.
(41) Loh, Z.-H.; Field, R. W. *J. Chem. Phys.* **2003**, *118*, 4037.
(42) Duan, Z.; Field, R. W.; Yamakita, N.; Tsuchiya, S. *Chem. Phys. Lett.* **2006**, *324*, 709.
(43) Wong, B. M.; Thom, R. L.; Field, R. W. *J. Phys Chem. A* **2006**, *110*, 7406.
(44) Wong, B. M.; Steeves, A. H.; Field, R. W. *J. Phys. Chem. B* **2006**, *110*, 18912.
(45) Layne, B. H.; Duffy, L. M.; Bechtel, H. A.; Steeves, A. H.; Field, R. W. *J. Phys. Chem. A* **2007**, *111*, 7398.
(46) Kellman, M. E. *J. Chem. Phys.* **1990**, *93*, 6630.
(47) Herman, M.; Liévin, J.; Vander Auwera, J.; Campargue, A. *Adv. Chem. Phys.* **1999**, *108*, 1.
(48) El Idrissi, M. I.; Zhilinskii, B.; P. Gaspard, P.; Herman, M. *Mol. Phys.* **2003**, *101*, 595.
(49) Zhilinskii, B. I.; El Idrissi, M. I.; Herman, M. *J. Chem. Phys.* **2000**, *113*, 7885.
(50) Vigouroux, C.; Fayt, A.; Guarnieri, A.; Huckauf, A.; Burger, H.; Lentz, D.; Preugschat, D. *J. Mol. Spectrosc.* **2000**, *202*, 1.
(51) Fayt, A.; Vigouroux, C.; Willaert, F.; Margules, L.; Constantin, L. F.; Demaison, J.; Pawelke, G.; El Bachir, M.; Buerger, H. *J. Mol. Struct.* **2004**, *695*−*696*, 295.
(52) Fayt, A.; Robert, S.; Di Lonardo, C.; Fusina, L.; Tamassia, F.; Herman, M. *J. Chem. Phys.* **2007**, *126*, 114303.
(53) Robert, S.; Herman, M.; Fayt, A.; Campargue, A.; Kassi, S.; Liu, A.; Wang, L.; Di Lonardo, G.; Fusina, L. *Mol. Phys.* **2008**, *106*, 2581.
(54) Robert, S.; Fayt, A.; Di Lonardo, G.; Fusina, L.; Tamassia, F.; Herman, M. *J. Chem. Phys.* **2005**, *123*, 174302/1.
(55) Cané, E.; Fusina, L.; Tamassia, F.; Fayt, A.; Herman, M.; Robert, S.; Vander Auwera, J. *Mol. Phys.* **2006**, *104*, 515.
(56) Di Lonardo, G.; Fusina, L.; Tamassia, F.; Fayt, A.; Robert, S.; Vander Auwera, J.; Herman, M. *Mol. Phys.* **2006**, *104*, 2617.
(57) Di Lonardo, G.; Fusina, L.; Tamassia, F.; Fayt, A.; Robert, S.; Vander Auwera, J.; Herman, M. *Mol. Phys.* **2008**, *106*, 1161.
(58) Brown, J. M.; Hougen, J. T.; Huber, K. P.; Johns, J. W. C.; Kopp, I.; Lefebvre-Brion, H.; Merer, A. J.; Ramsay, D. A.; Rostas, J.; Zare, R. N. *J. Mol. Spectrosc.* **1975**, *55*, 500.
(59) Robert, S.; Herman, M.; Vander Auwera, J.; Di Lonardo, G.; Fusina, L.; Blanquet, G.; Lepère, M.; Fayt, A. *Mol. Phys.* **2007**, *105*, 559.
(60) Di Lonardo, G.; Ferracuti, P.; Fusina, L.; Venuti, E.; Johns, J. W. C. *J. Mol. Spectrosc.* **1993**, *161*, 466.
(61) Di Lonardo, G.; Baldan, A.; Bramati, G.; Fusina, L. *J. Mol. Spectrosc.* **2002**, *213*, 57.
(62) Fusina, L.; Bramati, G.; Mazzavillani, A.; Di Lonardo, G. *Mol. Phys.* **2002**, *101*, 513.
(63) Zou, S.; Bowman, J. M.; Brown, A. *J. Chem. Phys.* **2003**, *118*, 10012.
(64) Tyng, V.; Kellman, M. E. *J. Phys. Chem. B* **2006**, *110*, 18859.
(65) Allen, W. D.; Yamaguchi, Y.; Császár, A. G.; Clabo, D. A., Jr.; Remington, R. B.; Schaefer, H. F., III. *Chem. Phys.* **1990**, *145*, 427.
(66) Martin, J. M. L.; Lee, T. J.; Taylor, P. R. *J. Chem. Phys.* **1998**, *108*, 676.
(67) Simmonett, A. C.; Schaefer, H. F., III; Allen, W. D. *J. Chem. Phys.* **2009**, *130*, 044301/1.
(68) Perevalov, B. V.; Kassi, S.; Romanini, D.; Perevalov, V. I.; Tashkun, S. A.; Campargue, A. *J. Mol. Spectrosc.* **2007**, *241*, 90.
(69) Perevalov, B. V.; Perevalov, V. I.; Campargue, A. *J. Quant. Spectrosc. Radiat. Transfer* **2008**, *109*, 2437.
(70) Perevalov, B. V.; Kassi, S.; Perevalov, V. I.; Tashkun, S. A.; Campargue, A. *J. Mol. Spectrosc.* **2008**, *252*, 143.
(71) Liu, A. W.; Kassi, S.; Perevalov, V. I.; Hu, S. M.; Campargue, A. *J. Mol. Spectrosc.* **2009**, *254*, 20.
(72) Law, M. M.; Duncan, J. L. *Chem. Phys. Lett.* **1993**, *212*, 172.

JP904000Q